J|A|C|S
ARTICLES
Published on Web 02/28/2004

Exceptionally Stable, Hollow Tubular Metal−Organic Architectures: Synthesis, Characterization, and Solid-State Transformation Study

Cheng-Yong Su,† Andrea M. Goforth, Mark D. Smith, P. J. Pellechia, and Hans-Conrad zur Loye*

Contribution from the Department of Chemistry and Biochemistry, University of South Carolina, Columbia, South Carolina 29208

Received October 13, 2003; E-mail: zurloye@mail.chem.sc.edu

Abstract: An effective solvothermal procedure has been developed to synthesize the new three-dimensional metal−organic framework, [ZnF(AmTAZ)]•solvents, using either 3-amino-1,2,4-triazole (AmTAZ) or 3-amino-1,2,4-triazole-5-carboxylic acid (AmTAZAc) and a choice of several Zn(II) salts as starting materials. The three-dimensional structure displays open-ended, hollow nanotubular channels that are formed by hexanuclear metallamacrocyclic $Zn_6F_6(AmTAZ)_6$ rings. The framework integrity is maintained to 350 °C, at which point most of the guest solvent molecules have been removed, as evidenced by single-crystal X-ray analyses, ^{1}H solid-state NMR, and TGA measurements. At higher temperatures, the framework is converted either to zinc oxide (ZnO) when heated in air or to zinc cyanamide ($ZnCN_2$) when heated in an inert atmosphere. In both cases, the as-grown, rodlike crystal shape is maintained during the solid-state transformation, suggesting a possible route for preparing one-dimensional crystalline nanomaterials.

Introduction

The design and synthesis of supramolecular architectures with open channel structures that contain pores of well-defined sizes, shapes, and chemical environments has attracted considerable attention from chemists, physicists, and materials scientists due to their potential applications in the areas of molecular sieves, sensors, gas absorption, ion exchange, size-selective separation, and heterogeneous catalysis.[1] Metal−organic frameworks constructed from metal ions and bridging organic ligands have afforded a promising approach toward the synthesis of open porous materials,[2] despite known difficulties, such as the inability to control pore size and shape, the existence of counterions and solvents within the channels, the interpenetration of independent networks, the disruption of framework integrity in the absence of guest molecules, and the often low thermal stability of the host framework. Consequently, current research has targeted the synthesis of robust open frameworks with high porosity and thermal stability,[3,4] and extensive studies have been carried out on chemical design strategies to enhance the desired properties of the frameworks. Successful approaches include the use of long rigid linkers to increase the spacing between the vertices,[5] employing multifunctional bulky organic ligands to prevent interpenetration,[6,7] and utilizing secondary building blocks (SBUs)[8] to serve as large vertices. This has created new challenges in the synthesis of tailored organic bridging ligands, in the judicious design of the functional SBUs, as well as in the efficient and synergistic self-assembly of these precursors to generate the desired framework structures.

Synthetic tubular architectures, which represent one type of open framework material, are of great interest because of their uniform, fixed internal diameters that can potentially enable their use in applications based on ion or molecular transport. In fact, significant progress has been made in the realm of organic nanotubular ensembles,[9] and open-ended, hollow nanotubes have

† Permanent address: School of Chemistry and Chemical Engineering, Zhongshan University, Guangzhou 510275, P. R. China.

(1) (a) Cheetham, A. K.; Férey, G.; Loiseau, T. *Angew. Chem., Int. Ed.* **1999**, *38*, 3269. (b) Eddaoudi, M.; Moler, D. B.; Li, H. L.; Chen, B. L.; Reineke, T. M.; O'Keeffe, M.; Yaghi, O. M. *Acc. Chem. Res.* **2001**, *34*, 319. (c) Hartgerink, J. D.; Clark, T. D.; Ghadiri, M. R. *Chem.-Eur. J.* **1998**, *4*, 1367. (d) Rao, C. N. R.; Nath, M. *Dalton Trans.* **2003**, 1. (e) Corma, A. *Chem. Rev.* **1997**, *97*, 2373. (f) Schüth, F.; Schmidt, W. *Adv. Mater.* **2002**, *14*, 629. (g) Stein, A. *Adv. Mater.* **2003**, *15*, 763.

(2) (a) Chui, S. S. Y.; Lo, S. M. F.; Charmant, J. P. H.; Orpen, A. G.; Williams, I. D. *Science* **1999**, *283*, 1148. (b) Hagrman, P. J.; Hagrman, D.; Zubieta, J. *Angew. Chem., Int. Ed.* **1999**, *38*, 2639. (c) Chen, B. L.; Eddaoudi, M.; Hyde, S. T.; O'Keeffe, M.; Yaghi, O. M. *Science* **2001**, *291*, 1021. (d) Gardner, G. B.; Venkataraman, D.; Moore, J. S.; Lee, S. *Nature* **1995**, *374*, 792.

(3) (a) Eddaoudi, M.; Kim, J.; Rosi, N.; Vodak, D.; Wachter, J.; O'Keefe, M.; Yaghi, O. M. *Science* **2002**, *295*, 469. (b) Noro, S.; Kitagawa, S.; Kondo, M.; Seki, K. *Angew. Chem., Int. Ed.* **2000**, *39*, 2082.

(4) Eddaoudi, M.; Li, H. L.; Yaghi, O. M. *J. Am. Chem. Soc.* **2000**, *122*, 1391.

(5) (a) Pschirer, N. G.; Ciurtin, D. M.; Smith, M. D.; Bunz, U. H. F.; zur Loye, H. C. *Angew. Chem., Int. Ed.* **2002**, *41*, 583. (b) Rosi, N. L.; Eddaoudi, M.; Kim, J.; O'Keeffe, M.; Yaghi, O. M. *Angew. Chem., Int. Ed.* **2001**, *41*, 284. (c) Biradha, K.; Hongo, Y.; Fujita, M. *Angew. Chem., Int. Ed.* **2000**, *39*, 3843.

(6) Xu, X. L.; Nieuwenhuyzen, M.; James, S. L. *Angew. Chem., Int. Ed.* **2002**, *41*, 764.

(7) (a) Yaghi, O. M.; Davis, C. E.; Li, G. M.; Li, H. L. *J. Am. Chem. Soc.* **1997**, *119*, 2861. (b) Goldberg, I. *Chem.-Eur. J.* **2000**, *6*, 3863.

(8) (a) Kim, J.; Chen, B. L.; Reineke, T. M.; Li, H. L.; Eddaoudi, M.; Moler, D. B.; O'Keeffe, M.; Yaghi, O. M. *J. Am. Chem. Soc.* **2001**, *123*, 8239. (b) Su, C. Y.; Yang, X. P.; Kang, B. S.; Mak, T. C. W. *Angew. Chem., Int. Ed.* **2001**, *40*, 1725. (c) Seo, J. S.; Whang, D.; Lee, H.; Jun, S. I.; Oh, J.; Jeon, Y. J.; Kim, K. *Nature* **2000**, *404*, 982. (d) Bourne, S. A.; Lu, J. J.; Mondal, A.; Moulton, B.; Zaworotko, M. J. *Angew. Chem., Int. Ed.* **2001**, *40*, 2111.

(9) (a) Bong, D. T.; Clark, T. D.; Granja, J. R.; Ghadiri, M. R. *Angew. Chem., Int. Ed.* **2001**, *40*, 988. (b) Gleiter, R.; Werz, D. B.; Raus, B. J. *Chem.-Eur. J.* **2003**, *9*, 2576.

10.1021/ja039022m CCC: $27.50

been created from cyclic peptides,[10] lipids,[11] oligocyclodextrins,[12] and other related organic systems.[13] Furthermore, interest in synthetic inorganic nanotubes was intensified by the discovery of carbon nanotubes,[14] and, subsequently, many functional inorganic nanotubes containing elements other than carbon (e.g., B, N, Si, O, S, and diverse metal ions) have been prepared.[15] The rapid development of this field has led to a general interest in one-dimensional nanomaterials[16] and has resulted in the fabrication of a wide variety of nanowires and nanorods.[17]

By contrast, coordination framework-based tubular structures are still in their infancy, although the methods for assembling metal−organic frameworks with high porosity are well established.[3−6] For example, linear coordination chains can form tubular architectures by coiling into hollow, helical conformations,[18] while the interweaving of two independent, undulating networks can lead to the serendipitous formation of nanotubes.[19] Other coordination framework-based tubular structures have been generated from judiciously designed multidentate ligands.[20] In this paper, an efficient and reliable solvothermal method for the fabrication of a new nanotubular metal−organic framework is described that uses the commercially available small ligands, 3-amino-1,2,4-triazole (AmTAZ) or 3-amino-1,2,4-triazole-5-carboxylic acid (AmTAZAc), and any one of a variety of Zn(II) salts as starting materials. The tubular framework is based on a hexanuclear $Zn_6F_6(AmTAZ)_6$ metallacycle repeating unit that is linked to form open-ended, hollow nanotubes. Each tube shares its single-layer wall with six neighboring ones to generate a three-dimensional (3D) honeycomb framework. This tubular framework exhibits extremely high thermal stability and maintains its crystal morphology and crystallinity even after the removal of the guest molecules from the channels. At high temperature, the metal−organic framework can be converted either to crystalline zinc oxide (ZnO) when heated in the presence of oxygen or to zinc cyanamide ($ZnCN_2$) when heated in an inert atmosphere. Interestingly, the original crystal shape is retained during the solid-state transformation, indicating a possible route for preparing 1D nanocrystalline materials from nanocrystalline metal−organic framework precursors.

Experimental Section

General Procedures. 3-Amino-1,2,4-triazole (AmTAZ) and 3-amino-1,2,4-triazole-5-carboxylic acid hemihydrate (AmTAZAc) were purchased from Research Chemical Ltd.; zinc(II) nitrate hexahydrate and zinc(II) tetrafluoroborate hydrate were purchased from Aldrich Chemical Co.; and zinc(II) fluoride tetrahydrate was purchased from Strem Chemicals. All chemicals and reagents were used as received without further purification. ^{1}H NMR spectra were collected at room temperature on a Varian Mercury/VX 300 spectrometer. Solid-state ^{1}H NMR spectra were recorded on a Varian Inova 500 spectrometer using a 4 mm Doty MAS probe at spin rates ranging from 0 to 15 kHz. Solid-state infrared spectra in the 4000−500 cm^{-1} region were recorded on a Shimadzu FTIR-8400 spectrophotometer using KBr as reference. Thermogravimetric analyses were carried out on a TA Instruments SDT 2960 simultaneous DTA−TGA by heating the samples at a rate of 5 °C/min under either flowing helium or air. Scanning electron microscopy (SEM) was performed on an ESEM FEI XL30 system. Energy-dispersive X-ray spectroscopy (EDS) was performed on an ESEM FEI Quanta 200 system. X-ray powder diffraction (XRD) patterns were acquired on a Rigaku D\Max-2200 powder X-ray diffractometer with graphite monochromatized Cu Kα radiation ($\lambda = 0.15418$ nm). The C, H, N, and F analyses were performed by Desert Analytics Laboratory.

Preparation of [ZnF(AmTAZ)]·Solvents. In a typical synthesis, 0.13 g (1 mmol) of AmTAZAc, 0.12 g (0.5 mmol) of zinc(II) tetrafluoroborate hydrate, and 0.09 g (0.5 mmol) of zinc(II) fluoride tetrahydrate were placed in a 23 mL Teflon liner; 4 mL of ethanol and 6 mL of water were then added. The resulting mixture was stirred for 5 min and was then sealed in a Parr autoclave. The autoclave was then placed in a programmable furnace and heated to 160 °C at 1 °C/min and held at that temperature for 30 h. The mixture was then cooled to 70 °C at 0.5 °C/min and kept at 70 °C for 10 h before the furnace was shut off. Colorless needle-shaped crystals formed. Yield: 60%. IR (KBr, cm^{-1}): 3456 (m), 3292 (m), 3217 (m), 3140 (w), 1622 (s), 1547 (s), 1521 (s), 1431 (m), 1315 (w), 1294 (m), 1064 (m), 885 (w), 754 (w), 653 (w). Anal. Calcd: C, 15.6; H, 3.1; N, 29.1; F, 9.9. Found: C, 15.9; H, 2.8; N, 28.7; F, 9.5, suggesting the formulation $(ZnFC_2H_3N_4)(CH_3CH_2OH)_{0.25}(H_2O)_{0.75}$. ^{1}H solid-state NMR: δ 1.411 (CH_3CH_2OH), 3.927 (CH_3CH_2OH), 4.428 (free H_2O), 8.937 (ligand−NH_2).

ZnF(AmTAZ)·solvents may also be prepared from other metal salts that serve as sources of Zn^{2+}, F^-, or both Zn^{2+} and F^-. Additionally, the AmTAZ ligand may be employed instead of AmTAZAc to construct the framework. The tubular framework can accommodate both ethanol and water molecules in various proportions depending on the solvent system used in the synthesis. Several reaction conditions leading to the formation of ZnF(AmTAZ)·solvents are summarized in Scheme 1.

Solid-State Transformation into ZnO. The as-prepared, colorless crystals of [ZnF(AmTAZ)]·solvents were loaded into an alumina boat which was placed in the center of a high-temperature tube furnace. The sample was heated in flowing air at a rate of 10 °C/min to 800 °C and maintained at this temperature for 2 h. A white product, which kept the same outer shape as the metal−organic precursor crystals, was identified as crystalline ZnO with the wurtzite structure by means of powder XRD and EDS.

(10) (a) Ghadiri, M. R.; Granja, J. R.; Milligan, R. A.; McRee, D. E.; Khazanovich, N. *Nature* **1994**, *372*, 709. (b) Ghadiri, M. R.; Granja, J. R.; Buehler, L. K. *Nature* **1994**, *369*, 301. (c) Sanchez-Ouesada, J.; Isler, M. P.; Ghadiri, M. R. *J. Am. Chem. Soc.* **2002**, *124*, 10004.

(11) (a) Karlsson, M.; Sott, K.; Davidson, M.; Cans, A. S.; Linderholm, P.; Chiu, D.; Orwar, O. *Proc. Natl. Acad. Sci. U.S.A.* **2002**, *99*, 11573. (b) Schüth, J. M. *Science* **1993**, *262*, 1669.

(12) (a) Harada, A.; Li, J.; Kamachi, M. *Nature* **1993**, *364*, 516. (b) Kraus, T.; Budesinsky, M.; Cisarova, I.; Zavada, J. *Angew. Chem., Int. Ed.* **2002**, *41*, 1715.

(13) (a) Fenniri, H.; Mathivanan, P.; Vidale, K. L.; Sherman, D. M.; Hallenga, K.; Wood, K. V.; Stowell, J. G. *J. Am. Chem. Soc.* **2001**, *123*, 3854. (b) Abrahams, B. F.; Hoskins, B. F.; Michail, D. M.; Robson, R. *Nature* **1994**, *369*, 727. (c) Hong, B. H.; Lee, J. Y.; Lee, C. W.; Kim, J. C.; Bae, S. C.; Kim, K. S. *J. Am. Chem. Soc.* **2001**, *123*, 10748. (d) Henze, O.; Lentz, D.; Schäfer, A.; Franke, P.; Schlüter, A. D. *Chem.-Eur. J.* **2002**, *8*, 357.

(14) (a) Iijima, S. *Nature* **1991**, *354*, 56. (b) Ajayan, P. M. *Chem. Rev.* **1999**, *99*, 1787.

(15) (a) Terrones, M.; Hsu, W. K.; Kroto, H. W.; Walton, D. R. M. In *Fullerenes and Related Structures*; Springer−Verlag Berlin: Berlin, 1999; Vol. 199, pp 189−234. (b) Suenaga, K.; Colliex, C.; Demoncy, N.; Loiseau, A.; Pascard, H.; Willaime, F. *Science* **1997**, *278*, 653. (c) Chopra, N. G.; Luyken, R. J.; Cherrey, K.; Crespi, V. H.; Cohen, M. L.; Louie, S. G.; Zettl, A. *Science* **1995**, *269*, 966. (d) Stephan, O.; Ajayan, P. M.; Colliex, C.; Redlich, P.; Lambert, J. M.; Bernier, P.; Lefin, P. *Science* **1994**, *266*, 1683. (e) Remskar, M.; Mrzel, A.; Skraba, Z.; Jesih, A.; Ceh, M.; Demšar, J.; Stadelmann, P.; Lévy, F.; Mihailovic, D. *Science* **2001**, *292*, 479. (f) Hacohen, Y. R.; Grunbaum, E.; Tenne, R.; Sloan, J.; Hutchison, J. L. *Nature* **1998**, *395*, 336.

(16) Xia, Y.; Yang, P.; Sun, Y.; Wu, Y.; Mayers, B.; Gates, B.; Yin, Y.; Kim, F.; Yan, H. *Adv. Mater.* **2003**, *15*, 353.

(17) (a) Han, W. Q.; Fan, S. S.; Li, Q. Q.; Hu, Y. D. *Science* **1997**, *277*, 1287. (b) Hu, J. T.; Odom, T. W.; Lieber, C. M. *Acc. Chem. Res.* **1999**, *32*, 435. (c) Hong, B. H.; Bae, S. C.; Lee, C. W.; Jeong, S.; Kim, K. S. *Science* **2001**, *294*, 348. (d) Patzke, G. R.; Krumeich, F.; Nesper, R. *Angew. Chem., Int. Ed.* **2002**, *41*, 2446.

(18) (a) Orr, G. W.; Barbour, L. J.; Atwood, J. L. *Science* **1999**, *285*, 1049. (b) Kaes, C.; Hosseini, M. W.; Rickard, C. E. F.; Skelton, B. W.; White, A. H. *Angew. Chem., Int. Ed.* **1998**, *37*, 920. (c) Cui, y.; Lee, S. J.; Lin, W. B. *J. Am. Chem. Soc.* **2003**, *125*, 6014.

(19) Jung, O.-S.; Kim, Y. J.; Kim, K. M.; Lee, Y.-A. *J. Am. Chem. Soc.* **2002**, *124*, 7906.

(20) (a) Aoyagi, M.; Biradha, K.; Fujita, M. *J. Am. Chem. Soc.* **1999**, *121*, 7457. (b) Hong, M. C.; Zhao, Y. J.; Su, W. P.; Cao, R.; Fujita, M.; Zhou, Z. Y.; Chan, A. S. C. *Angew. Chem., Int. Ed.* **2000**, *39*, 2468. (c) Kleina, C.; Graf, E.; Hosseini, M. W.; De Cian, A.; Fischer, J. *Chem. Commun.* **2000**, 239. (d) Daiguebonne, C.; Guillou, O.; Boubekeur, K. *Inorg. Chim. Acta* **2000**, *304*, 161. (e) Su, C.-Y.; Smith, M. D.; zur Loye, H.-C. *Angew. Chem., Int. Ed.* **2003**, *42*, 4085. (f) Fan, J.; Zhu, H. F.; Okamura, T. A.; Sun, W. Y.; Tang, W. X.; Ueyama, N. *Inorg. Chem.* **2003**, *42*, 158.

Scheme 1 [a]

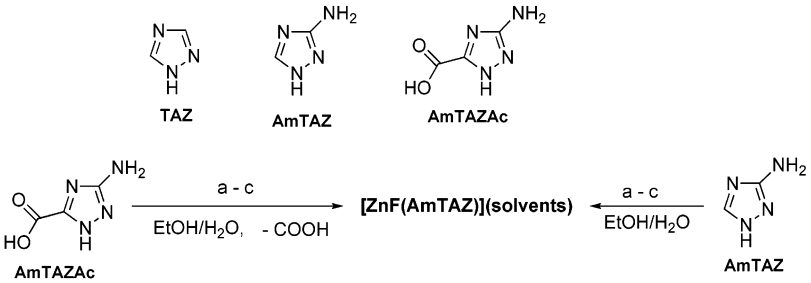

[a] (a) $Zn(BF_4)_2 + HNO_3$; (b) $Zn(NO_3)_2 + ZnF_2$; (c) $Zn(BF_4)_2 + ZnF_2$; (I) in $EtOH/H_2O$; (II) in H_2O; (III) in EtOH.

Solid-State Transformation into $ZnCN_2$. Crystals of [ZnF(AmTAZ)]·solvents were treated by the same procedure as that used to prepare nanocrystalline ZnO but were heated in flowing N_2 instead of flowing air. The N_2 flow was started 2 h before heating to expel trace oxygen left in the system. The resulting product was identified as zinc(II) cyanamide by means of powder XRD and EDS.

Crystal Structure Determination. Three low temperature data sets were collected using the same crystal. Data were collected on (a) the as-grown crystal obtained directly from the reaction, (b) the same crystal after heating it to 100 °C, and (c) the same crystal after heating it to 350 °C. For each data collection, the crystal was affixed to the tip of a glass fiber with a minimum of paratone-N oil and flash-frozen in the cold nitrogen stream of the diffractometer. The data collections were identical, covering reciprocal space with high redundancy to $2\theta = 56.6°$. The intensity data were measured at 150(2) K using a Bruker SMART APEX CCD-based diffractometer (Mo Kα radiation, $\lambda = 0.71073$ Å).[21] Raw data frame integration and Lp corrections were performed with SAINT+.[21] Final unit cell parameters are based on the least-squares refinement of all reflections from each data set with $I > 5(\sigma)I$. Analysis of each data set showed negligible crystal decay during collection. Empirical absorption corrections were applied with SADABS.[21] Systematic absences in the intensity data for each crystal were consistent with the space groups *R*3*c* and *R*-3*c*. The structures were solved in *R*-3*c* by a combination of direct methods and difference Fourier syntheses and were refined by full-matrix least-squares against F^2, using SHELXTL.[22] Refinement in *R*3*c* was also performed, but resulted in the same ligand and guest molecule disorder as was observed in *R*-3*c* (vide infra); *R*-3*c* was retained as the proper space group.

Refinement of each data set proceeded as follows: an initial solution from the as-grown crystal revealed a three-dimensional, channel-containing framework structure (see structure discussion). After identification of the framework species, multiple diffuse electron density peaks due to disordered guest molecules in the channels were observed. The distribution of these peaks was chemically featureless, and their identity or concentration could not be conclusively determined. They appear to be a mixture of ethanol and water, as discussed later. For the present refinements, they were modeled as variable occupancy oxygen atoms of water molecules. Difference peaks were added to the atom list until a flat difference map was achieved, and the largest residual electron density was located outside the channels (near Zn). A common fixed isotropic thermal parameter of $U_{eq} = 0.10$ Å^2 was assigned to all intrachannel oxygen atoms, and the occupancies were allowed to refine freely to the final values. This U_{eq} value was chosen after initially refining a common U_{eq} and subsequently fixing it near the final refined value. H atoms were not located or calculated for these species. All non-hydrogen atoms of the $ZnF(C_2H_3N_4)$ framework were refined with anisotropic displacement parameters; hydrogen atoms of the framework were calculated and included as riding atoms.

(21) *SMART Version 5.625, SAINT+ Version 6.02a and SADABS*; Bruker Analytical X-ray Systems, Inc.: Madison, WI, 1998.
(22) Sheldrick, G. M. *SHELXTL Version 5.1*; Bruker Analytical X-ray Systems, Inc.: Madison, WI, 1997.

Table 1. Crystal Data for As-Grown and Heated [ZnF(AmTAZ)]·Solvents

	as-grown (a)	100 °C (b)	350 °C (c)
empirical formula	$C_2H_3FN_4O_{1.65}Zn$	$C_2H_3FN_4O_{0.86}Zn$	$C_2H_3FN_4O_{0.16}Zn$
fw	193.83	181.14	169.94
cryst syst	trigonal	trigonal	trigonal
space group	*R*-3*c*	*R*-3*c*	*R*-3*c*
a (Å)	18.5059(7)	18.5486(7)	18.5744(7)
c (Å)	9.9168(7)	9.8538(7)	9.8413(7)
V (Å^3)	2941.2(3)	2936.0(3)	2940.4(3)
Z	18	18	18
ρ_{calc} (g cm^{-3})	1.970	1.844	1.727
T (K)	150(2)	150(2)	150(2)
μ (mm^{-1})	3.714	3.705	3.685
GOF	1.065	1.067	1.072
$\Delta\rho_{max,\ min}$	0.384, −0.383	0.422, −0.262	0.350, −0.286
R1[a]	0.0241	0.0233	0.0270
wR2[b]	0.0631	0.0636	0.0674

[a] $R1 = \sum ||F_o| - |F_c||/\sum|F_o|$. [b] $wR2 = [\sum w(F_o^2 - F_c^2)^2/\sum w(F_o^2)^2]^{1/2}$.

For data sets (b) and (c), the lattice parameters and symmetry indicated that the framework had survived the heating process unchanged. Therefore, the atomic coordinates from data set (a) were used for refinement of the data collected for the heated crystals. Rapid convergence indicated the framework was indeed unchanged. Guest molecules from (a) were not included in the refinements for (b) and (c), but were located from difference maps. The solvent peaks for (b) and (c) were assigned in the same manner as was done for (a).

A summary of the crystal data for (a)−(c) is given in Table 1. Selected bond distances and bond angles are listed in Table 2. Further details are presented in the Supporting Information.

Results and Discussion

Syntheses and Crystal Morphology. A simple synthetic procedure for preparing the 3D metal−organic framework, [ZnF(AmTAZ)]·solvents, was achieved via a solvothermal process. As shown in Scheme 1, a series of reactions all lead to the same target product, and general reaction conditions, including temperature, time, solvent medium, and heating or cooling rate, can be varied without affecting the identity of the reaction product. This generates a large number of viable synthetic conditions and enables the fine-tuning of the crystallization conditions to control both the crystal morphology and the particle size of the product (vide infra).

The ligand AmTAZAc was originally chosen for its multiple Lewis basic sites (the carboxylic acid group, the amino group, and the three imino-nitrogen atoms) with the intention of achieving the formation of a metal−organic framework via multiple bonding interactions. Unexpectedly, the ligand underwent decarboxylation to produce AmTAZ, indicating that the carboxylic acid group is unstable under the solvothermal conditions used. Decarboxylation was also observed for the related ligand 1,2,4-triazole-3-carboxylic acid, under similar

Table 2. Selected Bond Distances (Å) and Angles (deg)[a]

	As-Grown		
Zn−N(3)#1	1.998(2)	N(3)#1−Zn−N(2)	121.94(4)
Zn−N(2)	2.0177(15)	N(2)#2−Zn−N(2)	116.12(9)
Zn−F(1)	2.0814(8)	N(3)#1−Zn−F(1)	91.41(2)
C(1)−N(2)	1.317(2)	N(2)#2−Zn−F(1)	87.43(5)
C(1)−N(3)	1.348(2)	N(2)−Zn−F(1)	91.08(4)
C(1)−N(1)	1.400(3)	N(3)#1−Zn−F(1)#3	91.41(2)
N(2)−N(2)#5	1.394(3)	N(2)#2−Zn−F(1)#3	91.07(4)
Zn#4−F(1)−Zn	118.19(7)	N(2)−Zn−F(1)#3	87.43(5)
F(1)−Zn−F(1)#3	177.18(4)		
	100 °C		
Zn−N(3)#1	1.996(2)	N(3)#1−Zn−N(2)#2	122.19(4)
Zn−N(2)	2.0183(15)	N(2)#2−Zn−N(2)	115.62(9)
Zn−F(1)	2.0745(8)	N(3)#1−Zn−F(1)	91.89(2)
C(1)−N(2)	1.319(2)	N(2)#2−Zn−F(1)	87.41(5)
C(1)−N(3)	1.350(2)	N(2)−Zn−F(1)	90.57(4)
C(1)−N(1)	1.396(3)	N(3)#1−Zn−F(1)#3	91.89(2)
N(2)−N(2)#5	1.394(3)	N(2)#2−Zn−F(1)#3	90.57(4)
Zn#4−F(1)−Zn	118.42(7)	N(2)−Zn−F(1)#3	87.42(5)
F(1)−Zn−F(1)#3	176.23(4)		
	350 °C		
Zn−N(3)#1	1.996(3)	N(3)#1−Zn−N(2)	122.39(5)
Zn−N(2)	2.0205(18)	N(2)#2−Zn−N(2)	115.22(11)
Zn−F(1)	2.0704(9)	N(3)#1−Zn−F(1)	92.10(3)
C(1)−N(2)	1.320(3)	N(2)#2−Zn−F(1)	87.30(7)
C(1)−N(3)	1.353(3)	N(2)−Zn−F(1)	90.45(5)
C(1)−N(1)	1.388(4)	N(3)#1−Zn−F(1)#3	92.11(3)
N(2)−N(2)#5	1.392(3)	N(2)#2−Zn−F(1)#3	90.45(5)
Zn#4−F(1)−Zn	118.79(9)	N(2)−Zn−F(1)#3	87.30(7)
F(1)−Zn−F(1)#3	175.79(6)		

[a] Symmetry transformations used to generate equivalent atoms: #1 $y + {}^1/_3, -x + y + {}^2/_3, -z + {}^2/_3$; #2 $y, x, -z + {}^1/_2$; #3 $-y + {}^2/_3, x - y + {}^1/_3, z + {}^1/_3$; #4 $-x + y + {}^1/_3, -x + {}^2/_3, z - {}^1/_3$; #5 $-x + {}^2/_3, -x + y + {}^1/_3, -z + {}^5/_6$.

reaction conditions.[23] As a consequence of this decarboxylation, the same structure is obtained when using either AmTAZAc or AmTAZ as the ligand starting material. The framework [ZnF(AmTAZ)] is charge neutral because the two positive charges on the Zn^{2+} ion are balanced by one F^- anion and one deprotonated AmTAZ ligand.[24] Any of the following zinc(II)-containing salts can be used as the source of Zn^{2+} and/or of F^- as detailed in Scheme 1: ZnF_2, $Zn(NO_3)_2$, and $Zn(BF_4)_2$. Interestingly, the anions NO_3^- and BF_4^- do not participate in coordinating the Zn^{2+} cation, and they exert no apparent influence on the formation of the metal−organic framework. It is notable that $Zn(BF_4)_2$ can be used as the sole metal-containing reagent because it easily decomposes to release the F^- anion[28] in addition to providing a source of Zn^{2+}. Under certain reaction conditions, a white solid impurity was observed in addition to the main product and was identified as Zn(OH)F by X-ray powder diffraction.

(23) Wiley, D. W.; Webster, O. W.; Blanchard, E. P. *J. Org. Chem.* **1976**, *41*, 1889.
(24) Deprotonation of the 1,2,4-triazole ligand ($pK_a = 2.25$[25]) is found to be a common feature of its hydrothermal chemistry in the presence of metals, and a shift in pK_a is found to occur under hydrothermal conditions.[26] Therefore, it is understandable that AmTAZ ($pK_a = 4.04$[27]) takes the deprotonated form to participate in metal ion coordination under slightly acidic reaction conditions. The pH of a typical reaction mixture before reaction is about 4. The use of AmTAZAc may give a more acidic reaction mixture, but because it undergoes decarboxylation to become AmTAZ, deprotonation is still expected.
(25) Satchell, J. F.; Smith, B. J. *Phys. Chem. Chem. Phys.* **2002**, *4*, 4314.
(26) Chesnut, D. J.; Kusnetzow, A.; Birge, R.; Zubieta, J. *Inorg. Chem.* **1999**, *38*, 5484.
(27) Voronkov, M. G.; Kashik, T. V.; Makarskii, V. V.; Lopyrev, V. A.; Ponomareva, S. M.; Shibanova, E. F. *Dokl. Akad. Nauk SSSR* **1976**, *227*, 1116.
(28) van Konigsbruggen, P. J.; Hassnoot, J. G.; de Graaff, R. A. G.; Reedijk, J. *J. Chem. Soc., Dalton Trans.* **1993**, 483.

The consistent formation of the identical metal−organic framework is convincingly established by powder X-ray diffraction (XRD) measurements. The structural consistency and phase purity of each reaction were checked by comparison of the observed X-ray diffraction pattern with that calculated from the single-crystal structural data (see Figure S1). Thermogravimetric analysis (TGA) was carried out on the product of each reaction, and similar overall weight loss patterns were observed, although slight differences were noted in the onset temperature and magnitude of the first weight loss, which corresponds to the removal of some of the guest solvent molecules. By choosing different solvent compositions for the synthesis, the number and identity of the guest solvent molecules residing in the channels can be altered, which is the reason for the existence of slight variations in the elemental analysis results. Infrared spectra of all synthesized products display essentially identical absorption profiles, confirming that they contain the same chemical components and only differ due to the identity of the guest solvents located in the channels.

Microscopy can readily be used to ascertain the effect of the synthetic conditions on the crystal morphology. The crystals possess a rodlike outer appearance and can exist either as separated rods or as aggregated bundles of rods as shown in Figure 1. The size and clustering of the rodlike crystals was found to be closely tied to the specific reaction conditions. Syntheses using AmTAZAc typically resulted in well-separated, rodlike crystals, while syntheses using AmTAZ generally produced bundles of rodlike crystals. This observation is consistent with slower growth rates when AmTAZAc is used instead of AmTAZ; faster growth rates are expected for AmTAZ because the reaction to produce the framework does not require the additional decarboxylation step. Other reaction conditions, such as solvent medium, concentration, temperature, heating or cooling rate, Zn^{2+} and F^- sources, and even the inner surface of the Teflon liner, have profound influences on the crystal size and morphology. Although every single crystal possesses the same bar shape regardless of the reaction conditions, crystal size can range from nanometers to millimeters depending on the specific reaction conditions. Thus, precise synthetic control over crystal size is possible. In general, using AmTAZ leads to a better overall yield and greater product purity than does using AmTAZAc. Larger crystals are most readily obtained from AmTAZ, especially when the ethanol-to-water ratio is high and when lower reagent concentrations and longer times are utilized in the reaction.

Structure of [ZnF(AmTAZ)]·Solvents. X-ray single-crystal diffraction studies on the freshly synthesized compound revealed an extended, 3D nanotubular framework formulated as $(ZnFC_2H_3N_4)O_{1.65}$ where the oxygen atoms are located inside the tubular channels and deduced from multiple diffuse electron density peaks. Due to the severe disorder of the guest molecules in the channels, the distribution of these peaks was chemically featureless and the electron density was crystallographically modeled as ensuing from oxygen atoms of water molecules whose hydrogen atoms are neglected. Elemental microanalysis of crystals from the same batch suggested a formula of [ZnF(AmTAZ)]·$(C_2H_5OH)_{0.25}(H_2O)_{0.75}$ which closely matches the result of the structural analysis if the carbon atoms of ethanol are regarded as oxygen atoms. The presence of the ethanol

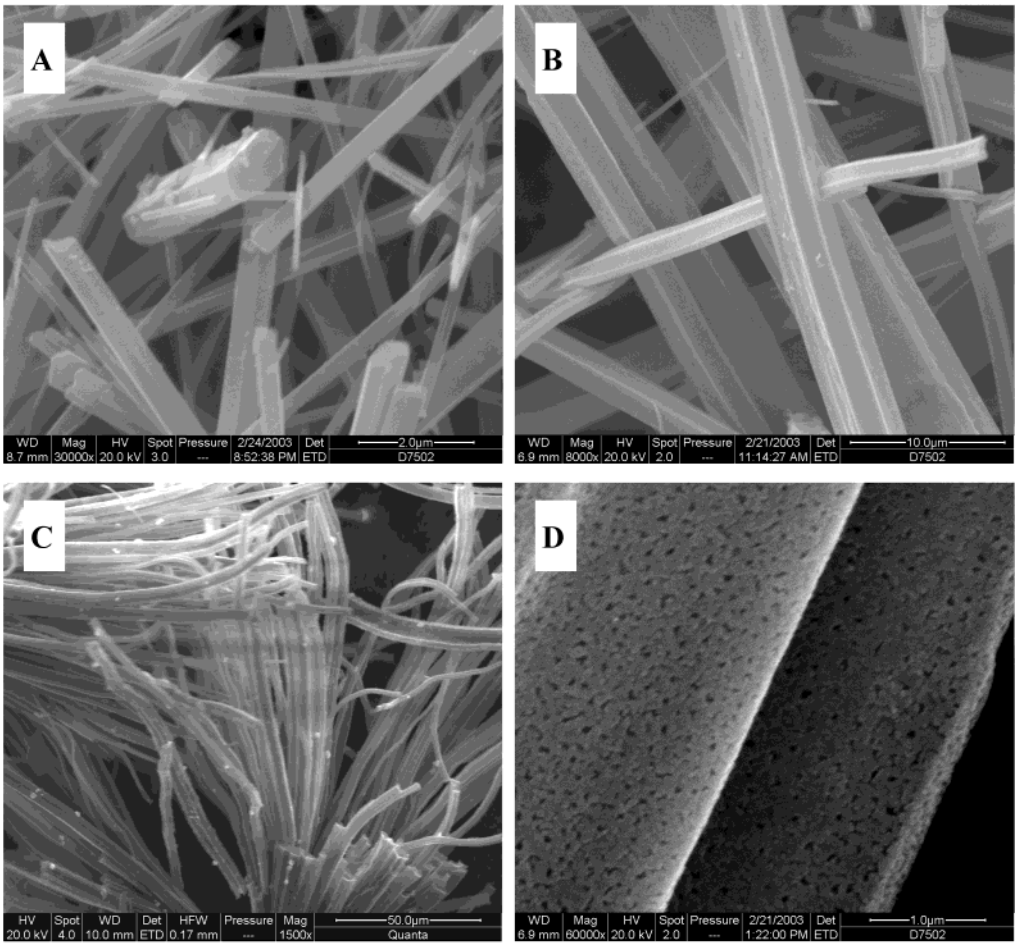

Figure 1. SEM micrographs of (a) the as-prepared metal−organic framework, (b) ZnO formed at elevated temperature in the presence of O_2, (c) $ZnCN_2$ formed at elevated temperature in the presence of N_2, and (d) a detailed surface feature of ZnO.

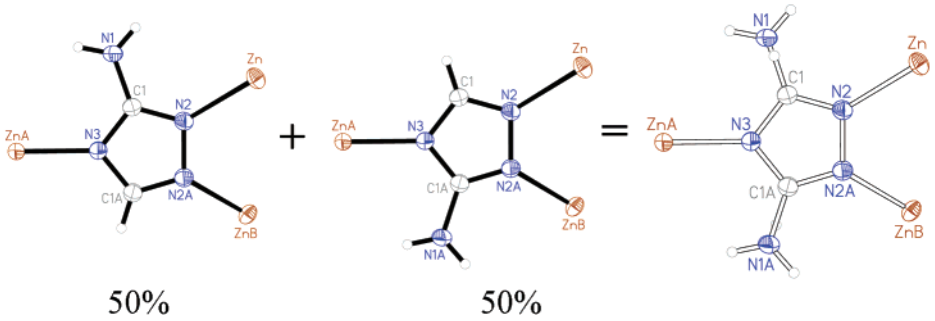

Figure 2. 50/50 ligand disorder about the two-fold axis (horizontal).

molecules in the channels was also confirmed by a ^1H NMR measurement, vide infra.

The skeleton of the framework consists of a fundamental repeating unit [ZnF(AmTAZ)], where the Zn and F atoms are located on two-fold rotational axes. The AmTAZ ligand is also located on a two-fold axis, causing a two-fold disorder of this ligand throughout the crystal structure as shown in Figure 2 (for clarity, only one ligand disorder component is shown in most of the following figures). As depicted in Figure 3, each Zn^{2+} center has a trigonal bipyramidal geometry with the three equatorial sites occupied by an imino-nitrogen atom from three separate AmTAZ ligands and the two apical positions occupied by F^- anions. All three nitrogen atoms in the triazole (TAZ) ring are coordinated to different Zn^{2+} centers, and the Zn^{2+} centers are further connected by F^- anions that act as μ_2-bridging atoms to link two neighboring Zn^{2+} centers. Thus, propagation of the structure in the crystal involves the μ_3-TAZ units and the μ_2-F^- anions to generate a 3D framework containing very large hexagonal channels as shown in Figure 4. Unfortunately, the amino group of the AmTAZ ligand protrudes into these channels, reducing their effective diameter.

Figure 5a clearly shows the framework structure surrounding a single channel. The framework can be viewed as consisting of open-ended, hollow tubes extending along the *c*-axis with a crystallographically imposed $\bar{3}$ axis lying in the center of each tube. Consequently, as shown in Figure 5b, each tube consists of hexanuclear metallamacrocycles made up of six AmTAZ units and six Zn^{2+} metal centers that are related by three-fold rotoinversion symmetry. Within this metallamacrocycle, each AmTAZ ligand utilizes its 1- and 4-positioned nitrogen donors

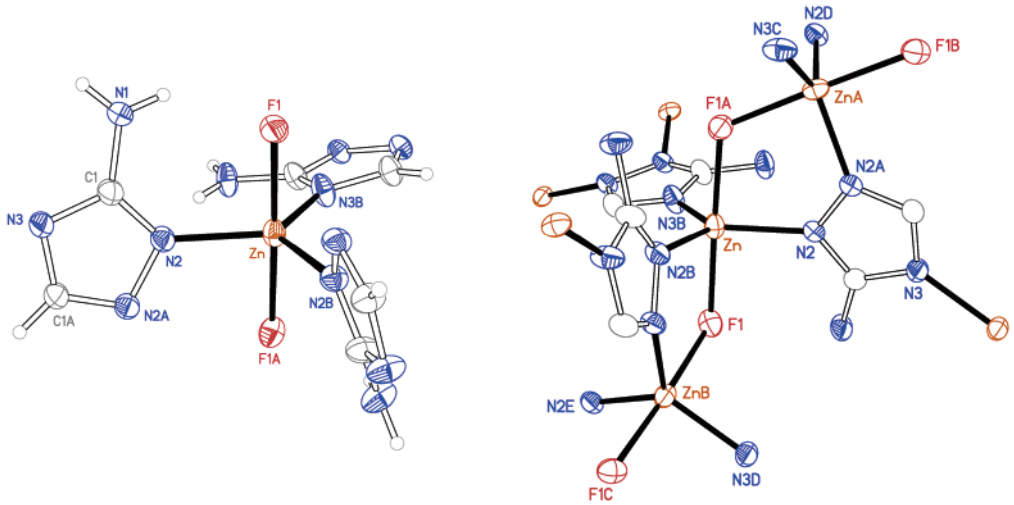

Figure 3. ORTEP drawing with atom-labeling scheme of the zinc(II) coordination environment (left) and linkage between adjacent zinc(II) ions (right). The atoms are drawn as thermal ellipsoids at the 50% probability level.

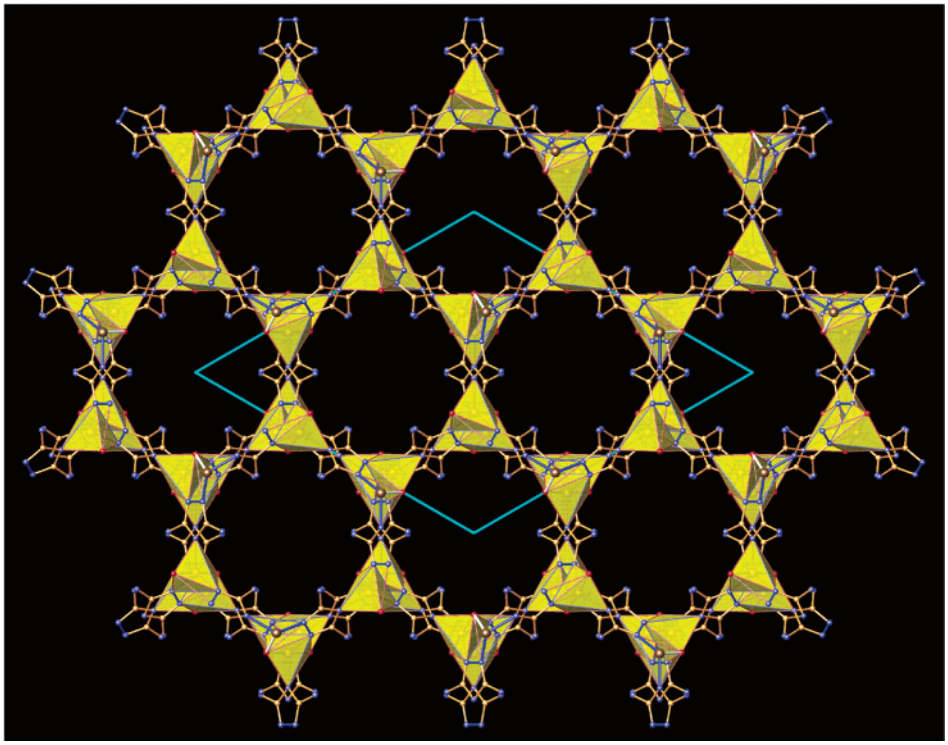

Figure 4. Honeycomb tubular channels formed in the [ZnF(AmTAZ)] framework along the *c*-axis. The coordination geometry of the zinc(II) centers is represented by golden trigonal bipyramids. The AmTAZ ligands are shown in the two-fold disordered mode. Hydrogen atoms and guest molecules are omitted for clarity. Key: Zn, bronze; F, red; N, blue; C, yellow.

to link two five-coordinate Zn^{2+} metal ions through two of the three equatorial sites. Each Zn^{2+} ion is further coordinated to another AmTAZ ligand with N−Zn−N angles of 121.94° (Table 2), enabling the formation of $\bar{3}$-symmetry related metallmacrocycles. Fusing of these metallamacrocycles via the third bridging AmTAZ ligand results in the honeycomb arrangement observed in the *ab* plane (Figure 4). In addition, the 2-positioned nitrogen donor of each AmTAZ ligand is bound to one of the six Zn^{2+} centers belonging to an adjacent, eclipsing hexanuclear metallamacrocycle. As shown in Figure 5c, stacking of such metallamacrocycles in an eclipsed configuration results in 1D chains running along the *c*-axis where connectivity is established via vertex sharing of ZnN_3F_2 polyhedra. Adjacent Zn centers in these chains are part of five-membered Zn_2N_2F rings, where each ring is composed of the two Zn centers, a μ_2-bridging F^- anion, and the 1- and 2-positioned bridging nitrogen atoms of an AmTAZ ligand. Overall, the AmTAZ unit utilizes its 1- and 4-positioned nitrogen atoms to link trigonal bipyramidal Zn^{2+} centers into metallamacrocycles that are fused to generate a 2D honeycomb sheet in the *ab* plane. Such 2D sheets are connected in the third direction via bridging F^- anions and 2-positioned AmTAZ nitrogen atoms to generate the 3D honeycomb tubular framework.

The cylindrical channels of the tubular framework possess hydrophilic internal cavities, as the amino group of the AmTAZ ligand points into the channels. These amino groups reduce the effective diameter of the tubes and restrict the movement of guest molecules. The channels have a 12 × 12 Å cross section;

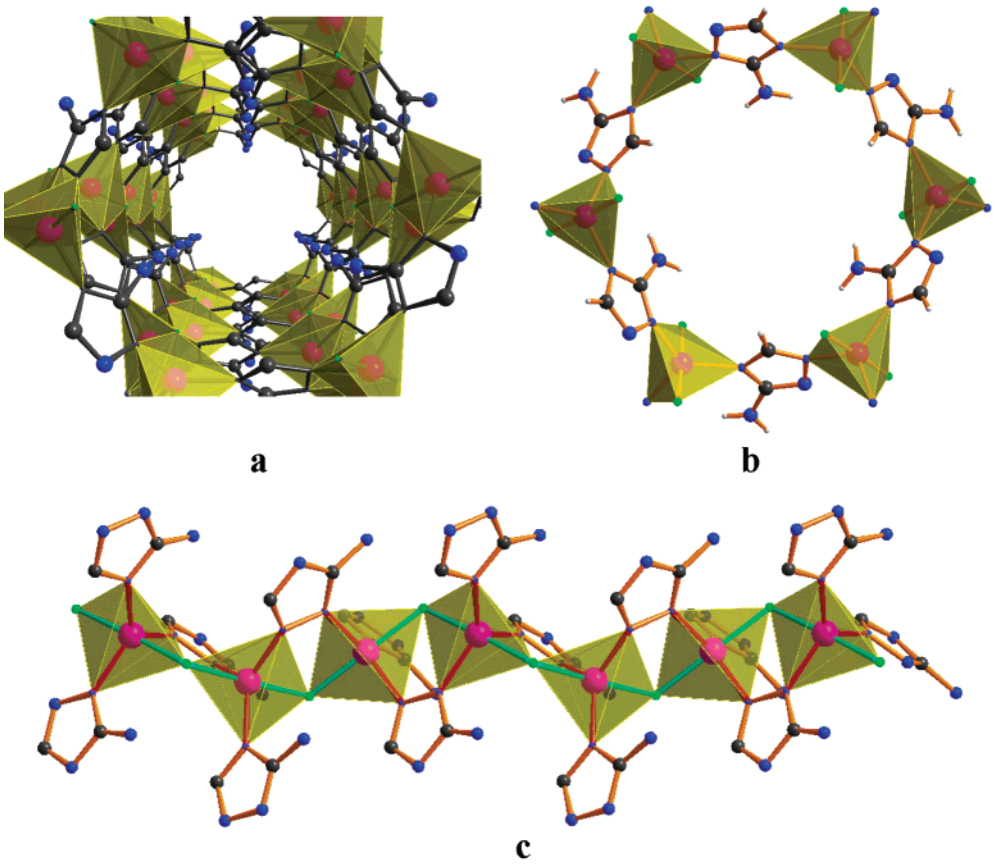

Figure 5. (a) Perspective view of the open-ended, hollow nanotube. (b) Three-fold symmetry related hexanuclear metallamacrocycle composed of six AmTAZ and six zinc(II) centers. (c) 1D chain containing five-membered Zn_2N_2F rings resulting from eclipsed stacking of $Zn_6F_6(AmTAZ)_6$ metallamacrocycles. The coordination geometry of the zinc(II) centers is represented by golden trigonal bipyramids. Key: Zn, purple; F, green; N, blue; C, black; H, gray.

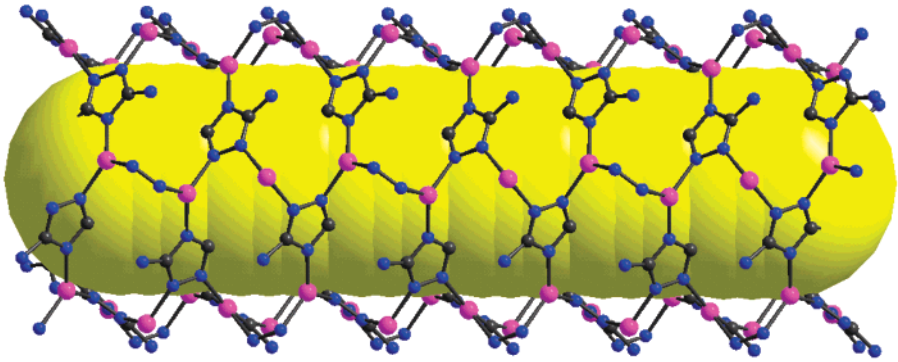

Figure 6. Tubular structure of each channel showing the compact single-layer wall made up of μ_3-AmTAZ ligands. The tube interior is represented by a yellow cylinder in contact with the AmTAZ ligands. Fluorine and hydrogen atoms are omitted for clarity.

however, taking the van der Waals radii (1.7, 1.5, 1.2 Å for C, N, and H, respectively) into account, the aperture may only admit the passage of a sphere with a 5 Å diameter. The total solvent-accessible volume of the channel in the unit cell is 741.6 $Å^3$, which accounts for 25.2% of the total cell volume as calculated by PLATON.[29] While a 25% solvent-accessible volume is significant, it is smaller than that found in some high porosity metal−organic frameworks constructed using long linkers or large SBUs.[2−6] One reason for this relatively smaller value is that the channels are nonintersecting in [ZnF(AmTAZ)]. This situation is quite different in other porous metal−organic frameworks having diamondoid or cubic topologies, which can contain intersecting channels and hence have a larger interior volume. In [ZnF(AmTAZ)], the wall of each tube consists of a "single layer" that is formed by μ_3-AmTAZ ligands connected via Zn^{2+} ions as shown in Figure 6. While these nonintersecting channels restrict the movement of guest molecules to one direction, this structural motif does appear to enhance the thermal stability of the framework, as removal of guest molecules at temperatures up to 375 °C does not result in framework decomposition.

Guest Removal and Structural Robustness and Integrity. As mentioned earlier, it is possible to influence which guest solvent molecules are lodged in the channels by selecting the solvent system during the synthesis step. Although the high mobility of these guest molecules makes their characterization difficult by single-crystal X-ray analysis, their identity can be

(29) Spek, A. L. *Acta Crystallogr.* **1990**, *A46*, C34.

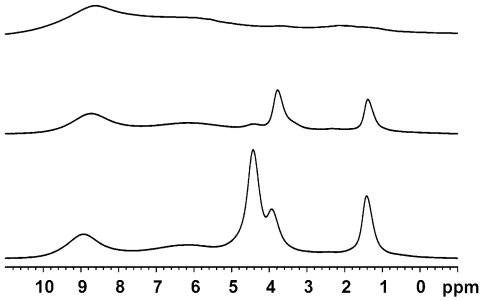

Figure 7. ^{1}H solid-state NMR for freshly prepared [ZnF(AmTAZ)]·$(C_2H_5OH)_{0.25}(H_2O)_{0.75}$ (bottom), after heat treatment at 250 °C for 1 h (middle), and after heat treatment at 350 °C for 1 h (top).

confirmed by ^{1}H NMR measurements. Solution ^{1}H NMR spectra do not provide any information on the ligand itself because of the insolubility of the framework; however, the existence of ethanol guests in frameworks synthesized in ethanolic solutions was confirmed by observing the ethanol proton signals in a deuterated solution in which the framework was placed and heated for a few minutes. This observation suggests that the ethanol molecules in the channels can be replaced by other small solvent molecules.

In addition to solution measurements, ^{1}H solid-state NMR measurements were carried out on the as-synthesized and heated samples. The spectrum acquired without sample spinning displayed only a broad signal around 4.4 ppm due to the large dipolar interactions between protons; however, the spectra acquired at high spin rates showed well-resolved proton signals as shown in Figure 7. The two peaks at 1.411 ppm ($-CH_3$) and 3.927 ppm ($-CH_2$) in the spectrum of the as-synthesized sample are attributed to ethanol, the intense peak at 4.428 ppm is believed to be due to water molecules, and the broad peak at 8.937 ppm is tentatively assigned to the $-NH_2$ group of AmTAZ (a fairly broad signal around 6.19 ppm is also observed which might correspond to the proton on the 5-position of the TAZ ring).[30] Upon heating the as-synthesized sample to 250 °C for 1 h in air, the peak assigned to water decreased dramatically and the peaks assigned to ethanol were also reduced in intensity, suggesting that most of the water and a portion of the ethanol were removed from the channels. Upon heating the sample to 350 °C for another hour, most of the ethanol was removed from the channels. Because the amino group of the AmTAZ ligand points into the channels, it is expected that some of the guest molecules may form N−H···O hydrogen bonds, which would hinder them from leaving the channels. It is, however, surprising that the ethanol molecules are harder to remove than the water molecules. One plausible explanation for this observation is that the tubular channels do not allow tumbling of the larger ethanol molecules, thereby slowing their diffusion out of the channels relative to the smaller water molecules.

A similar phenomenon was also observed in the thermogravimetric measurements. Figure 8a shows the TGA−DTA curves of a portion of a freshly prepared sample (the same sample as was used for elemental analysis) heated in flowing air, while Figure 8b shows the TGA−DTA curves of a different portion of the same sample heated in flowing helium after a 2 h purge period. In air, a small weight loss (5%, designated as A) occurred immediately upon heating and was completed before the temperature reached 100 °C, and this weight loss is indicative of the loss of non-hydrogen bonded solvent molecules. These non-hydrogen bonded solvent molecules are already removed from the channels in the dry He atmosphere during the purge cycle, as evidenced by the absence of the weight loss A (Figure 8b). In addition, a continuous, gradual weight loss (labeled B) is observed, which ceased at about 380 °C, and is followed by framework decomposition as indicated by an abrupt weight loss (labeled C). The total weight loss of guest molecules is about 12% and closely matches the solvent amount calculated from the formula [ZnF(AmTAZ)]·$(C_2H_5OH)_{0.25}(H_2O)_{0.75}$, which is based on the elemental analysis results (13%). It is worth mentioning that the removed guest molecules can be reintroduced into the channels. After being heated to 350 °C, the sample was soaked in an EtOH−H_2O mixture for 2 days, and the thermogravimetric measurements were repeated. Essentially the same weight loss occurs; however, this time, most of the guest molecules are removed before the temperature reaches 100 °C.

Another intriguing observation is that the crystals preserve their structure and crystallinity until they start to decompose above 380 °C. While we cannot demonstrate conclusively that the framework is solvent-free by 350 °C, optical microscopy was used to demonstrate that the crystals retain their transparency, crystallinity, and morphology on heating to 350 °C. To confirm the retention of crystallinity, one single crystal was subjected to the following three X-ray diffraction analyses: (a) measurement of the as-prepared single crystal, (b) measurement of the crystal after heating it to 100 °C, and (c) measurement of the crystal after heating it to 350 °C. As can be seen from Tables 1 and 2, the single-crystal X-ray analyses on the heated crystal yielded the same structure with lattice parameters and symmetry consistent with the as-synthesized sample. All bond distances and angles were essentially unchanged, illustrating the high stability, structural rigidity, and integrity of the metal−organic framework. Detailed analysis of the electron density peaks due to disordered guest molecules (see crystal structure determination) revealed the approximate amount of the solvent molecules left in the channels. Using exactly the same treatment method for the three data sets collected, a reliable comparison of the guest occupancy has been obtained. If all of the solvent peaks are modeled as ensuing from oxygen atoms of water molecules whose hydrogen atoms are neglected, the resulting oxygen content per Zn atom is (a) 1.65, (b) 0.86, and (c) 0.16. Due to the fact that we cannot unambiguously identify the channel guests and due to the high correlation between the displacement parameters and site occupancies for these guests, the preceding results are intended only to provide a qualitative measure of the trend in guest molecule content in the channels as a function of crystal heating. These experiments, however, demonstrate the retention of the sample crystallinity and the robustness of the metal−organic framework after prolonged and repeated heating and evacuation of the guest molecules. It is worth pointing out that, while a high thermal stability of porous metal−organic frameworks is a desired quality for application purposes, it is rarely achieved. Among the known frameworks with high thermal stability,[4,31] the single-crystal structure data communicated in this paper are, to the best of our knowledge,

(30) (a) Gil, A. M.; Alberti, E.; Parreira, C.; Goodfellow, B. J.; Rakvin, B. *J. Mol. Struct.* **2002**, *602*−*603*, 357. (b) Yamauchi, K.; Kuroki, S.; Fujii, K.; Ando, I. *Chem. Phys. Lett.* **2000**, *324*, 435. (c) Yamauchi, K.; Kuroki, S.; Ando, I. *J. Mol. Struct.* **2002**, *602*−*603*, 9.

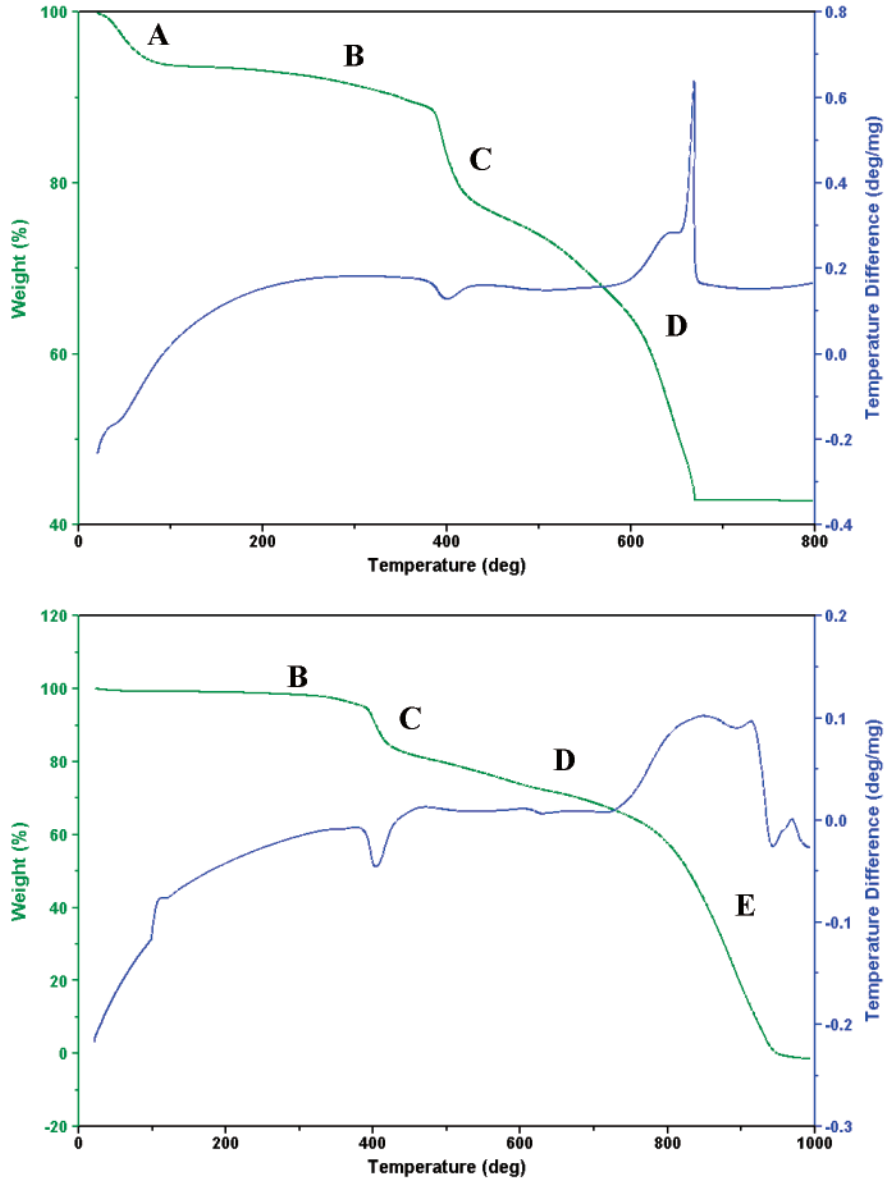

Figure 8. TGA−DTA curves for [ZnF(AmTAZ)]·solvent measured in flowing air (top) and helium (bottom).

those collected after the highest temperature treatment (350 °C). Prior to this work, Yaghi's MOF-5 framework held this distinction, having been heat-treated at 300 °C.[32]

Solid-State Transformation. As shown in Figure 8, TGA curves recorded in either air or helium flow exhibited a similar, abrupt weight loss (C) between 380 and 430 °C immediately following guest molecule removal. However, significantly different weight loss behavior was observed above 430 °C in the two different gaseous environments. In flowing air, the TGA curve showed a gradual weight loss (D) until 670 °C followed by a plateau at 42 wt % remaining. In flowing helium, on the other hand, the TGA curve showed a smooth weight loss (D) between 430 and 800 °C followed by a massive weight loss (E) ending at about 950 °C and zero weight %. To clarify the structural and chemical change in each case, powder X-ray diffraction (XRD) was used to follow this solid-state transformation as a function of temperature. The freshly prepared crystals of [ZnF(AmTAZ)]·solvents were placed in an alumina crucible and placed in the TGA analyzer. The temperature was increased at a rate of 5 °C/min in flowing air or helium. XRD patterns were collected after heating the sample at multiple, increasing temperatures until a single phase was obtained. Energy-dispersive spectroscopy (EDS) was employed to qualitatively determine the composition of the solid at each step.

As shown in Figure 9a, the XRD patterns for samples heated in flowing air at 230 and 350 °C remain unchanged, indicating that the structural integrity of the framework is maintained. This observation is in agreement with the previously discussed single-crystal structure results. When heated to 385 °C, the XRD pattern of the sample exhibits line broadening and decreased peak intensity, indicative of the beginning of a structural transformation and consistent with the appearance of an endothermic peak in the DTA (Figure 8a) at this temperature. Increasing the temperature to 400 °C results in the formation

(31) (a) Yaghi, O. M.; Li, G. M.; Li, H. L. *Nature* **1995**, *378*, 703. (b) Lu, J. Y.; Babb, A. M. *Chem. Commun.* **2002**, 1340. (c) Liu, Y. H.; Tsai, H. L.; Lu, Y. L.; Wen, Y. S.; Wang, J. C.; Li, K. L. *Inorg. Chem.* **2001**, *40*, 6426. (d) Liu, Y. H.; Lu, Y. L.; Wu, H. C.; Wang, J. C.; Lu, K. L. *Inorg. Chem.* **2002**, *41*, 2592.

(32) Li, H.; Eddaoudi, M.; O'Keeffe, M.; Yaghi, O. M. *Nature* **1999**, *402*, 276.

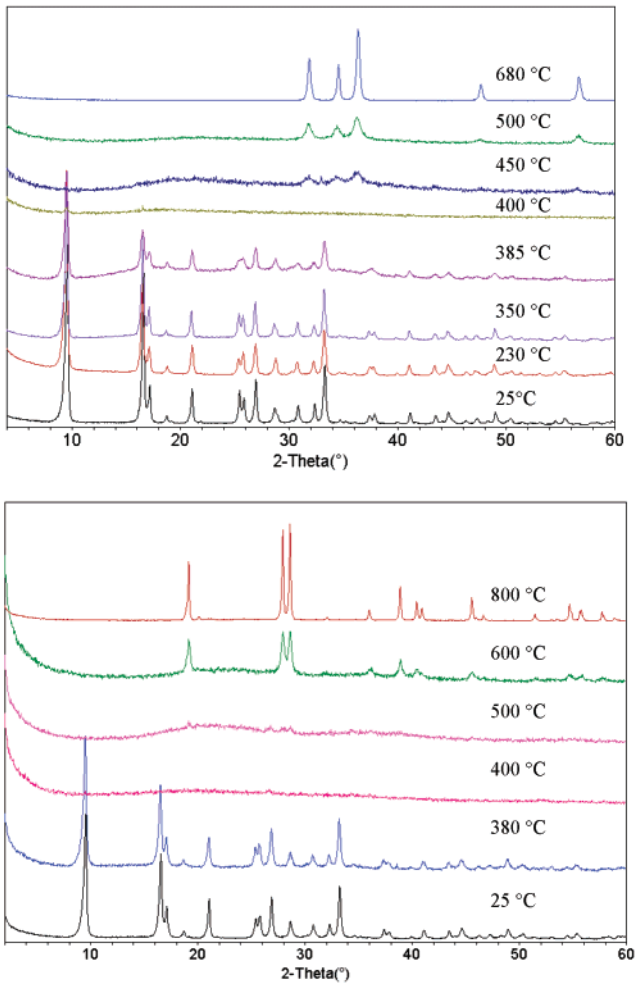

Figure 9. X-ray powder diffraction profiles of [ZnF(AmTAZ)]·solvent after heat treatment in flowing air (top) and dry nitrogen (bottom).

of an amorphous solid as illustrated by the absence of peaks in the XRD pattern. EDS analysis of this solid, which was kept at 400 °C for 30 min, revealed that all of the fluorine atoms had been removed from the as-synthesized compound (Figure S2a,b). This is consistent with the TGA measurement in which the sharp weight loss between 380 and 430 °C accounts for about 10 wt % and closely matches the calculated amount of 9.9% based on the formulation $[ZnF(AmTAZ)]\cdot(C_2H_5OH)_{0.25}(H_2O)_{0.75}$. After release of fluorine, the amorphous solid begins to crystallize as shown by the appearance of new diffraction peaks in the XRD pattern recorded after heating the sample to 450 °C. Meanwhile, the TGA displayed a continuous weight decrease until the temperature reached about 680 °C. These findings suggest that a new crystalline phase forms while the framework falls apart. A marked exothermic peak in the DTA in this temperature region is supportive of this suggestion. Finally, a single phase crystallized above 600 °C as shown in Figure 9a. This new product accounts for approximately 43% of the total sample weight, in good agreement with the formation of ZnO, which is calculated at 42.3%. The unambiguous characterization of the product is accomplished by a combination of EDS, which shows the presence of only Zn and O (Figure S2c), and XRD, which identifies the product as ZnO with the wurtzite structure (space group *P*63*mc*, PDF79-0206) as illustrated in Figure S3.[33]

Heating the sample in helium rather than oxygen leads to the formation of zinc cyanamide rather than zinc oxide. As before, we observe the retention of sample crystallinity up to 380 °C, followed by a rapid transformation to an amorphous solid accompanied by fluorine elimination. This transformation is then followed by the appearance of a new crystalline phase. As depicted in Figures 8b and 9b, a slow structural change accompanied by a gradual weight loss occurs above 430 °C. XRD measurements revealed the appearance of a new, crystalline phase between 500 and 800 °C, which is identified as zinc cyanamide, $ZnCN_2$ (tetragonal space group $I\text{-}42d$),[34] Figure S4. An EDS analysis of the solid heated to 500 and 800 °C in He confirms that only Zn, N, and C are present in the sample. The formation of $ZnCN_2$ requires a completely oxygen-free atmosphere; the existence of even trace amounts of oxygen leads to the cocrystallization of ZnO and $ZnCN_2$, as shown in Figure S5 where the XRD pattern contains the diffraction peaks characteristic of both ZnO and $ZnCN_2$.

Regardless of whether the sample is heated in air or in an inert atmosphere, an important finding is that, although the framework decomposes and the chemical composition changes, the intrinsic shape of the as-synthesized crystals is retained during the structure transformation. As shown in Figure 1, both ZnO and $ZnCN_2$ maintain the hexagonal rodlike morphology of the metal−organic precursor. This is of interest with respect to the potential of fabricating 1D nanostructures.[16] ZnO possesses interesting electronic, acoustic, and optical properties,[35] and its potential application in nanodevices has stimulated research to fabricate 1D ZnO nanostructures with diverse morphologies.[36] As a result, many synthetic methods including vapor-phase transport, high-temperature physical evaporation, template-induced methods, and recently established wet-chemical approaches have been applied toward ZnO nanoparticle synthesis.[37] Furthermore, $ZnCN_2$ has been used to prepare

(33) Albertsson, J.; Abrahams, S. C.; Kvick, A. *Acta Crystallogr.* **1989**, *B45*, 34.
(34) Becker, M.; Jansen, M. *Acta Crystallogr.* **2001**, *C57*, 347.
(35) (a) Ali, H. A.; Iliadis, A. A.; Mulligan, R. F.; Cresce, A. V. W.; Kofinas, P.; Lee, U. *Solid-State Electron.* **2002**, *46*, 1639. (b) Clarke, D. R. *J. Am. Ceram. Soc.* **1999**, *82*, 485. (c) Natsume, Y.; Sakata, H. *J. Mater. Sci.: Mater. Electron.* **2001**, *12*, 87. (d) Zhou, H.; Hofstaetter, A.; Hofmann, D. M.; Meyer, B. K. *Microelectron. Eng.* **2003**, *66*, 59. (e) Ng, H. T.; Chen, B.; Li, J.; Han, J. E.; Meyyappan, M.; Wu, J.; Li, S. X.; Haller, E. E. *Appl. Phys. Lett.* **2003**, *82*, 2023. (f) Studenikin, S. A.; Golego, N.; Cocivera, M. *J. Appl. Phys.* **1998**, *83*, 2104. (g) Rode, K.; Anane, A.; Mattana, R.; Contour, J. P.; Durand, O.; LeBourgeois, R. *J. Appl. Phys.* **2003**, *93*, 7676.
(36) (a) Vayssieres, L. *Adv. Mater.* **2003**, *15*, 464. (b) Guo, L.; Ji, Y. L.; Xu, H. B.; Simon, P.; Wu, Z. Y. *J. Am. Chem. Soc.* **2002**, *124*, 14864. (c) Tian, Z. R. R.; Voigt, J. A.; Liu, J.; McKenzie, B.; McDermott, M. J. *J. Am. Chem. Soc.* **2002**, *124*, 12954. (d) Park, W. I.; Kim, D. H.; Jung, S. W.; Yi, G. C. *Appl. Phys. Lett.* **2002**, *80*, 4232. (e) Pacholski, C.; Kornowski, A.; Weller, H. *Angew. Chem., Int. Ed.* **2002**, *41*, 1188. (f) Wang, Y. C.; Leu, I. C.; Hon, M. H. *J. Mater. Chem.* **2002**, *12*, 2439. (g) Yang, P. D.; Yan, H. Q.; Mao, S.; Russo, R.; Johnson, J.; Saykally, R.; Morris, N.; Pham, J.; He, R. R.; Choi, H. J. *Adv. Funct. Mater.* **2002**, *12*, 323. (h) Zhang, J.; Sun, L. D.; Pan, H. Y.; Liao, C. S.; Yan, C. H. *New J. Chem.* **2002**, *26*, 33. (i) Hu, P.; Liu, Y. Q.; Wang, X. B.; Fu, L.; Zhu, D. B. *Chem. Commun.* **2003**, 1304.
(37) (a) Liu, B.; Zeng, H. C. *J. Am. Chem. Soc.* **2003**, *125*, 4430. (b) Dai, Z. R.; Pan, Z. W.; Wang, Z. L. *Adv. Funct. Mater.* **2003**, *13*, 9. (c) Gorla, C. R.; Emanetoglu, N. W.; Liang, S.; Mayo, W. E.; Lu, Y.; Wraback, M.; Shen, H. *J. Appl. Phys.* **1999**, *85*, 2595. (d) Haupt, M.; Ladenburger, A.; Sauer, R.; Thonke, K.; Glass, R.; Roos, W.; Spatz, J. P.; Rauscher, H.; Riethmüller, S.; Müller, M. *J. Appl. Phys.* **2003**, *93*, 6252. (e) Huang, M. H.; Wu, Y. Y.; Feick, H.; Tran, N.; Weber, E.; Yang, P. D. *Adv. Mater.* **2001**, *13*, 113. (f) Kong, Y. C.; Yu, D. P.; Zhang, B.; Fang, W.; Feng, S. Q. *Appl. Phys. Lett.* **2001**, *78*, 407. (g) Wu, J. J.; Liu, S. C. *Adv. Mater.* **2002**, *14*, 215. (h) Yao, B. D.; Chan, Y. F.; Wang, N. *Appl. Phys. Lett.* **2002**, *81*, 757. (i) Lakshmi, B. B.; Patrissi, C. J.; Martin, C. R. *Chem. Mater.* **1997**, *9*, 2544. (j) Liu, J.; Lin, Y. H.; Liang, L.; Voigt, J. A.; Huber, D. L.; Tian, Z. R.; Coker, E.; McKenzie, B.; McDermott, M. J. *Chem.-Eur. J.* **2003**, *9*, 605. (k) Wang, Z.; Li, H. L. *Appl. Phys. A: Mater. Sci. Process.* **2002**, *74*, 201. (l) Sun, X. M.; Chen, X.; Deng, Z. X.; Li, Y. D. *Mater. Chem. Phys.* **2003**, *78*, 99.

nitrogen-containing carbon tubes via pyrolysis reactions.[38] The work presented in this paper offers a versatile preparation method for the metal−organic precursor, [ZnF(AmTAZ)]·solvents, which can be transformed into ZnO or $ZnCN_2$ rods that exhibit reasonable mechanical robustness. Furthermore, because the hexagonal rodlike crystal shape of the precursor is retained during the solid-state transformation, the resultant size of the ZnO or $ZnCN_2$ rods is fixed by the size of the metal−organic precursor crystals. This clearly suggests a promising approach to fabricate 1D inorganic ZnO and $ZnCN_2$ nanomaterials by an easy and straightforward method.

Conclusion

Construction of a nanotubular, 3D metal−organic framework, [ZnF(AmTAZ)]·solvents, has been successfully achieved by a flexible solvothermal route. The crystal morphology of the product and the identity of the guest solvent molecules encapsulated in its channels are adjustable subject to the choice of reaction conditions. The metal−organic framework itself is of interest with respect to the following aspects: (a) the 3D structure displays channels in a honeycomb arrangement; (b) the channels exhibit an open-ended, hollow tubular feature; (c) the tubes have a cylindrically compact single-layer wall constituted of tightly held AmTAZ, F^-, and Zn^{2+} ions; (d) the solvent molecules in the channels can be removed without collapse of the framework; (e) the framework exhibits high robustness and thermal stability; (f) the crystals possess a hexagonal rodlike morphology; and (g) the metal−organic framework turns into shape-preserved ZnO or $ZnCN_2$ when heated in air or an inert atmosphere, respectively. The unusual retention of the hexagonal rodlike morphology of the as-grown crystals during the solid-state transformation suggests a potential approach for fabricating 1D inorganic nanomaterials from metal−organic precursors.

A key contribution to all of the above features is the compact tubular topology of the metal−organic framework, which is based on the simple AmTAZ ligand. Because the amino group of AmTAZ points into the channels, creating a hydrophilic inner environment, the effective diameter of the tubes is reduced to about 5 Å. A potential way to sidestep this issue is to use the TAZ (TAZ = 1,2,4-triazole) ligand instead of AmTAZ during the synthesis, where a preliminary investigation has indicated that a similar tubular framework, one that lacks the amino groups inside the channels, can be created. A more hydrophobic inner environment and a larger diameter of the tube are expected with the TAZ ligand. A detailed investigation is ongoing and will be published soon.

Acknowledgment. We acknowledge the donors of the Petroleum Research Fund, administered by the American Chemical Society, for partial support through grant PRF#36822 and the National Science Foundation for partial support through grant CHE-0314164.

Supporting Information Available: XRD patterns of [ZnF(AmTAZ)]·solvent, ZnO, $ZnCN_2$, and their single-crystal diffraction simulations. Comparison of XRD patterns of ZnO, $ZnCN_2$, and a mixture of ZnO−$ZnCN_2$. EDS analyses of as-synthesized compound and the solids obtained by heating at different temperatures in air or He (PDF). X-ray crystallographic files in CIF format. This material is available free of charge via the Internet at http://pubs.acs.org.

JA039022M

(38) Becker, M.; Bender, H.; Jansen, M.; Kienle, L.; Assenmacher, W. *J. Phys. Chem. Solids* **2001**, *62*, 1431.